HHS Public Access

Author manuscript

Breast Cancer Res Treat. Author manuscript; available in PMC 2016 November 01.

Published in final edited form as:

Breast Cancer Res Treat. 2015 November ; 154(2): 251–262. doi:10.1007/s10549-015-3618-6.

Photodynamic therapy as an effective therapeutic approach in MAME models of inflammatory breast cancer

Neha Aggarwal[1], **Ann Marie Santiago**[2], **David Kessel**[2], and **Bonnie F. Sloane**[2,3]

Neha Aggarwal: naggarwa@med.wayne.edu; Ann Marie Santiago: asandago@med.wayne.edu; David Kessel: dhkessel@med.wayne.edu; Bonnie F. Sloane: bsloane@med.wayne.edu

[1]Department of Physiology, Wayne State University School of Medicine, 540 East Canfield, Detroit, MI 48201, USA

[2]Department of Pharmacology, Wayne State University School of Medicine, 540 East Canfield, Detroit, MI 48201, USA

[3]Department of Oncology, Wayne State University School of Medicine, 540 East Canfield, Detroit, MI 48201, USA

Abstract

Photodynamic therapy (PDT) is a minimally invasive, FDA-approved therapy for treatment of endobronchial and esophageal cancers that are accessible to light. Inflammatory breast cancer (IBC) is an aggressive and highly metastatic form of breast cancer that spreads to dermal lymphatics, a site that would be accessible to light. IBC patients have a relatively poor survival rate due to lack of targeted therapies. The use of PDT is underexplored for breast cancers but has been proposed for treatment of subtypes for which a targeted therapy is unavailable. We optimized and used a 3D mammary architecture and microenvironment engineering (MAME) model of IBC to examine the effects of PDT using two treatment protocols. The first protocol used benzoporphyrin derivative monoacid A (BPD) activated at doses ranging from 45 to 540 mJ/cm^2. The second PDT protocol used two photosensitizers: mono-L-aspartyl chlorin e6 (NPe6) and BPD that were sequentially activated. Photokilling by PDT was assessed by live–dead assays. Using a MAME model of IBC, we have shown a significant dose–response in photokilling by BPD–PDT. Sequential activation of NPe6 followed by BPD is more effective in photokilling of tumor cells than BPD alone. Sequential activation at light doses of 45 mJ/cm^2 for each agent resulted in >90 % cell death, a response only achieved by BPD–PDT at a dose of 360 mJ/cm^2. Our data also show that effects of PDT on a volumetric measurement of 3D MAME structures reflect efficacy of PDT treatment. Our study is the first to demonstrate the potential of PDT for treating IBC.

Correspondence to: Neha Aggarwal, naggarwa@med.wayne.edu.

Electronic supplementary material: The online version of this article (doi:10.1007/s10549-015-3618-6) contains supplementary material, which is available to authorized users.

Authors' Contributions NA carried out the experiments. AMS provided technical support with experiments. NA, DK, and BFS made substantial contributions to concept and design of experiments as well as drafting and/or revising the manuscript.

Compliance with ethical standards: Competing Interests: The authors declare that they have no competing interests.

Keywords

Inflammatory breast cancer; Photodynamic therapy; 3D; MAME cultures

Introduction

Inflammatory breast cancer (IBC) is a rare and highly malignant form of invasive breast carcinoma in which cancer cells form emboli that metastasize to the dermal lymphatic vasculature [1–6]. IBC has poorer prognosis than all other breast cancer subtypes with no targeted therapies for treatment. IBC is characterized by erythema, edema, and/or peau d'orange with or without a palpable mass in the breast. These symptoms along with blockage of lymphatic vasculature cause swelling of the breast, hence the name IBC. Epidemiologic studies have indicated that IBC is a heterogeneous disease [7, 8]. The expression of molecular markers in IBC differs depending on patient population; for example, Egyptian IBC patients have higher expression of RhoC GTPase than do patients from Tunisia, Morocco, and the USA [7, 8]. Conventional therapies (surgery, radiation, chemotherapy) alone or in combination are less effective against IBC than other breast cancers with the 3-year relative survival rate being only 42 % as compared to 85 % [1]. There are no targeted therapies for treatment of IBC [9–11].

Photodynamic therapy (PDT) is a treatment that involves three components: (1) a photosensitizer that preferentially localizes primarily in sub-cellular organelles of neoplastic cells, (2) dissolved oxygen in cells and tissues, and (3) light to activate the photosensitizer. The photosensitizer termed benzoporphyrin derivative monoacid A (BPD, Verteporfin™) localizes mainly to mitochondria, whereas mono-L-aspartyl chlorin e6 (NPe6) shows preferential affinity for lysosomes. When these photosensitizers are activated with light, the resulting photochemistry leads to the formation of potentially lethal reactive oxygen species [12–16]. An essential component to successful PDT is accessibility of the tumors to light. PDT has been shown to be effective in treating head and neck, esophageal, oral, laryngeal, and lung cancers [17, 18]. PDT has also been successful in treatment of chest wall metastases in end-stage breast cancer patients, prolonging survival [19–21]. We suggest that PDT may have the potential to eradicate the dermal metastases that are characteristic of IBC.

Recent reports using cells cultured in 2D indicate that use of two PSs (i.e., combination PDT) significantly increased cell death [22–24]. Studies from the Kessel laboratory have shown that sequential targeting of lysosomes followed by mitochondria promoted photokilling via apoptosis in a 2D murine hepatoma model [23]. Cells cultured in 2D do not, however, recapitulate the cellular architecture, that is, critical for accurately modeling tumor growth and response to therapies [25, 26]. In contrast, 3D models predict resistance to chemo- and radiation therapies [27–29]. Hasan and colleagues have adapted ovarian and pancreatic cancer cells to 3D models to evaluate PDT in photokilling these resistant cancer cells [30–32]. The 3D MAME culture model developed in our laboratory mimics in vivo architecture and allows studies of cell–cell interactions over time. These MAME models are being used to study drug responses ([33], Sameni et al., submitted) and the involvement of the tumor microenvironment and proteolysis in malignant progression [34–39]. Here we use

an IBC MAME model to demonstrate the efficacy of PDT including increased efficacy upon sequentially targeting lysosomes and mitochondria.

Methods

Tissue culture

SUM149 cells (a kind gift from Dr. Steven Ethier, MUSC) were used as a model of human IBC. Cells were maintained in 2D in Dulbecco's Modified Eagles Medium/Ham's F-12 (Sigma-Aldrich) supplemented with 5 % FBS (Hyclone), 5 μg/ml insulin (Sigma-Aldrich), 1 μg/ml hydrocortisone (Sigma-Aldrich), and 1 % Mycozap Plus-CL (Lonza). The invasive human TNBC breast cancer cell lines, MDA-MB-231 and Hs578T, were purchased from ATCC. MDA-MB-231 cells were maintained in medium composed of DMEM supplemented with 10 % FBS, 4 mM L-glutamine, and 1 % MycoZap plus-CL. Hs578T cells were cultured and maintained in DMEM medium supplemented with 10 % FBS, 5 μg/ml insulin, 4 mM L-glutamine, and 1 % MycoZap plus-CL. All cell lines were maintained in T-25 flasks in a humidified incubator (5 % CO_2) at 37 °C.

For some experiments, the SUM149 cells were transduced to express red fluorescent protein (RFP). Briefly, 50,000 cells were seeded in a 6-well dish and transduced with 20 μl cignal RFP viral particles (Qiagen). Transduced cells were flow sorted using the BD FACS vantage cell sorter to select the population of cells that expressed RFP. The SUM149-RFP cell line was maintained in 2D as described above for the wild-type cells.

Generation of MAME model of breast cancer cells

A reconstituted basement membrane (rBM) overlay model, developed by Bissell and colleagues [40–42], modified by Brugge and colleagues [43, 44], and adapted for multiple breast cancer cell lines by our laboratory [36, 38, 45], was used for all the experiments. To generate MAME models, glass coverslips (12 mm) were placed in 35-mm dishes and coated with 50 μl rBM (Cultrex, Trevigen). The rBM was allowed to gel for 15 min at 37 °C before seeding 5000 cells resuspended in 50 μl mammary epithelial cell growth medium (MEGM) medium [composed of mammary epithelial basal medium and MEGM SingleQuot kit supplements and growth factors (Lonza)]. After incubation at 37 °C for an hour to allow cells to adhere, an overlay of MEGM containing 2 % rBM was added and 3D structures were allowed to form for 6–7 days.

Photodynamic therapy

BPD-PDT—MAME cultures were incubated for 60 min at 37 °C with 1.5 μM BPD, washed with PBS, and replenished with overlay media. Cells were irradiated using a 700-watt quartz-halogen lamp and an interference filter that confines the irradiation to 690 ± 10 nm at a power density of 1.5 mW/cm^2. Irradiation was performed using light doses from 45 to 540 mJ/cm^2; this corresponds to time intervals ranging from 30 s to 6 min. Two controls were used: a protocol that results in 100 % killing and a dark control [46]. Following irradiation, samples were incubated at 37 °C for 18–24 h before live/dead assays were performed.

Combination PDT using BPD and NPe6—SUM149 cells were grown in MAME cultures for 7 days. On day 7, cultures were incubated with 1.5 μM BPD and/or 40 μM NPe6 for 60 min. Then the cells were irradiated with light at 690 nm (to initiate photodynamic effects of BPD) and/or at 660 nm (to initiate photodynamic effects of NPe6); see the figures for light doses. The sequential treatments are represented as NPe6/BPD when NPe6 was activated before BPD and BPD/NPe6 when BPD was activated before NPe6. Following irradiation, samples were incubated at 37 °C for approximately 24 or 48 h before live/dead assays were performed.

Live–dead assays

The live–dead assay kit (Life Technologies) has two components. A dye calcein AM (CG) that fluoresces green when cleaved by intracellular esterases is used to identify live cells. A second dye, ethidium homodimer-1 (EB), exhibits red fluorescence when incorporated into the DNA of dead cells. Cells were incubated with assay reagents for 30 min at 37 °C and washed once with warm PBS, and then warm MEGM media were added, and the cells were imaged live on a Zeiss 510 LSM META NLO confocal microscope using a 20× water-immersion objective. Z-stacks through entire structures were captured for 16 contiguous fields in at least three separate experiments (each such image takes 40–60 min to capture). The images were reconstructed in 3D and are represented here as either extended depth of focus images (*en face* view) or volume rendered 3D images tilted at a 45° angle using Volocity software. The green and red fluorescence intensities were quantified for each image. Cell viability was calculated as described by Celli et al. [46] and converted to percentage of dark controls and plotted against the PDT dose.

Methods for assessing apoptosis

Cleaved Caspase-3 Immunofluorescence—SUM149 cells were grown in MAME cultures and treated on day 7 using the sequential NPe6/BPD PDT protocol at a dose of 22.5 mJ/cm^2. MAME structures were then fixed at 6, 12, and 24 h post-PDT using 4 % paraformaldehyde for 20 min, washed 3 times with PBS, and permeabilized with 0.2 % Triton X-100 for 5 min followed by quenching three times with 0.1 M glycine for 10 min. Non-specific binding sites were then blocked with 0.2 % BSA for 60 min. Samples were incubated overnight at 4 °C with a 1:400 dilution of cleaved caspase-3 antibody (Cell Signaling Technology). The samples were then washed four times with PBS for 10 min each. The cells were then treated with a 1:1000 dilution of AlexaFluor 488 (Life Technologies) for an hour at room temperature and washed four times with PBS for 10 min each, and the samples were imaged on the Zeiss 510 LSM META NLO confocal microscope using a 40× water-immersion objective. The z-stack images were quantified to determine the intensity of cleaved caspase-3 and reconstructed in 3D using Volocity software.

Nuclear staining with Hoechst—SUM149 cells were grown in MAME cultures for 7 days and treated with the sequential NPe6/BPD–PDT protocol at a dose of 22.5 mJ/cm^2; 24 h later, a 1:1000 dilution of Hoechst dye HO33342 was added for 15 min. The medium was replaced and MAME structures were imaged live on a Zeiss 510 LSM META NLO confocal microscope using a 40× water-immersion objective. The images were reconstructed in 3D to show an extended depth of focus images (*en face* view) using Volocity software.

Statistics

Statistical significance was determined using GraphPad Prism 6.0 software. Experiments were analyzed using multiple comparison *t* test, one-way or two-way ANOVA as stated for each experiment.

Results

3D MAME structures exhibit a dose–response to photokilling by BPD–PDT

We utilized a MAME model of IBC to assess the dose–response to a PDT protocol in which mitochondria are targeted using BPD. Approximately 50 % of 3D structures were killed at a 45 mJ/cm^2 BPD–PDT dose. When we increased the light dose, there was a progressive decrease in cell viability (Fig. 1, Table 1), ultimately resulting in a 95 % photokilling effect at a light dose of 540 mJ/cm^2. Thus, there was a significant increase in death of IBC MAME structures in response to escalating the BPD–PDT dose.

At the molecular level, breast cancer is characterized based on expression of hormone receptors [estrogen receptor (ER) and progesterone receptor (PR) and the amplification of the human epidermal growth factor receptor type 2 (HER2)]. The most lethal cancers are characterized by the absence of ER, PR, and HER2 over-expression and designated triple-negative breast cancers (TNBCs). Due to limited commercial availability of models for IBC, most experiments were performed with the SUM149 IBC cell line, which is also a TNBC cell line [38, 47]. We also analyzed the efficacy of PDT for two commercially available non-IBC TNBC cell lines: MDA-MB-231 (Fig. 2) and Hs578T (Supplemental Fig. 1). Increases in doses of BPD–PDT resulted in a significant dose–response in photokilling of MDA-MB-231 and Hs578T MAME structures. At the lowest BPD–PDT dose (45 mJ/cm^2), there were ∼15 and 18 % cell deaths in MDA-MB-231 and Hs578T 3D structures, respectively. At the highest BPD–PDT dose (540 mJ/cm^2), ∼6 and 73 % cell deaths in MDA-MB-231 and Hs578T 3D structures, respectively, were observed. These data demonstrate the efficacy of PDT in photokilling MAME structures of TNBCs and suggest that PDT may be useful for treating TNBC chest wall metastases that would be easily accessible to light.

Combination PDT promotes photokilling of IBC structures in MAME model

Next, we assessed the cytotoxic response of combining two photosensitizers that target two critical organelles within a cell, mitochondria, and lysosomes, using BPD and NPe6, respectively. These photosensitizing agents differ in their absorbance spectra, and so photodamage with each agent can be separately initiated [23]. We examined the effects on photokilling of the order of activation of the photosensitizers at three doses (Fig. 3, Table 2, Supplemental Fig. 2).

At a PDT dose of 22.5 mJ/cm^2, we observed a significant difference in photokilling in response to the order of irradiation of the mitochondrial targeted PS and the lysosomal targeted PS (Fig. 3a–c, Supplemental Fig. 2a). Cell death with BPD was 19 % and with NPe6 was 5 %. The response to a combination of BPD and NPe6 was greater than additive compared to either alone. A sequential protocol of irradiation at 690 nm followed by 660 nm, resulted in 35 % cell death. In contrast, a sequential protocol of 660 nm irradiation

followed by 690 nm irradiation yielded 57 % photokilling. Thus, targeting lysosomes before mitochondria resulted in enhanced photokilling efficacy for IBC MAME structures.

Kessel and Reiners [23] developed a protocol for photokilling involving NPe6 and BPD, which resulted in a greatly enhanced degree of photokilling, using a 2D model of 1c1c7 hepatoma cells. Based on this study, we chose a light dose of 45 mJ/cm^2 for NPe6 and 22.5 mJ/cm^2 for BPD (Fig. 3d–f, Table 2, Supplemental Fig. 2b). In our IBC MAME model, cell death resulting from BPD alone was ∼12 % and with NPe6 alone 27 %. A sequential protocol targeting either mitochondria or lysosomes first resulted in ∼60 % cell death. A two-fold difference in light doses when targeting mitochondria first did, however, results in an increase in photokilling by 25 % compared to the effect of a light dose of 22.5 mJ/cm^2 (for both BPD and NPe6) (see Table 2).

Using a light dose of 45 mJ/cm^2, we observed a substantial degree of photokilling, with the order of activation of the photosensitizers not being significant (Fig. 3g–i, Table 2, Supplemental Fig. 2c). Cell death with either BPD or NPe6 was 36 and 44 %, respectively. We observed a significant increase in cell death using sequential protocols targeting mitochondria first or lysosomes first, i.e., cell deaths of 81 and 94 %, respectively. If lysosomes are targeted first, all IBC MAME structures were eradicated at a light dose of 45 mJ/cm^2.

Changes in volume of IBC MAME structures indicate response to combination PDT

A decrease in tumor burden is used as a standard measure of response to anti-tumor therapy. In this respect, mathematical algorithms for 3D modeling of patient tumors and prediction of surgical volume better assess breast tumor stage and response to therapies [48, 49]. The volume of nasopharyngeal carcinoma rather than their size is associated with poorer survival and faster recurrence [50–52]. Here we measured the volume of MAME structures to determine if this parameter could be used to quantify response to combination PDT (Fig. 4). We observed an increase in size and volume of MAME structures over a period of 4 days for the dark controls (Fig. 4a–e). In contrast, there was significant decrease in the size and volume of MAME structures over the 4 days following NPe6/BPD treatment at a light dose of 22.5 mJ/cm^2 (Fig. 4a′–e′). These data suggest that the volumetric measurement of MAME structures can be used as an indirect method to evaluate response to therapy.

Apoptosis is the mechanism of cell death following combination PDT

PDT targeting either mitochondria or lysosomes results leads to the initiation of apoptosis, an irreversible route to cell death [12, 14–16, 53–59]. Morphologic features associated with apoptosis include cell shrinkage, dense cytoplasm, chromatin condensation (pyknosis), and nuclear fragmentation (karyorrhexis) [60–62]. The apoptotic process is very tightly regulated; however, once executioner caspases (i.e., caspases-3, 6 or 7) are activated, a cell is destined to undergo programmed cell death [62–66]. We observed a time-dependent increase in activated caspase-3 as a result of NPe6/BPD treatment at a dose of 22.5 mJ/cm^2 (Fig. 5a, b). By 24 h post-PDT, nuclear fragmentation and chromatin condensation were present (Fig. 5c). The activated caspase-3 and changes in nuclear morphology observed here in response to sequential PDT protocol are consistent with cell death occurring by apoptosis.

Calcium and metabolic byproducts such as cytokines that are released by necrotic cells can damage the neighboring cells due to a bystander effect [67–70]. In contrast, apoptosis initiated by low-dose PDT does not initiate a bystander effect or immune response because toxic metabolites are not leaked from apoptotic cells [69, 70]. Here we evaluated the response to a low PDT dose of 22.5 mJ/cm^2 in IBC MAME models at one and two days following PDT. We observed that photokilling was similar on days 1 and 2 post combination PDT, which would be consistent with the absence of a bystander effect (Supplemental Fig. 3).

Discussion

IBC and TNBCs are lethal subtypes of breast cancer for which there are no targeted therapies. The usual treatment for these subtypes of breast cancer is chemotherapy followed by mastectomy and radiation with the prognosis poor. TNBC accounts for about 20–40 % of IBC cases and 15–20 % of non-IBC breast cancers [47, 71]. PDT has not yet been evaluated for treatment of IBC or its dermal metastases. The success of PDT in treating chest wall recurrences of breast cancer [19, 20] suggests that it will be efficacious against the dermal metastases of IBC. To our knowledge, this study is the first to show that PDT is an effective modality for photokilling of IBC structures in MAME models. 3D models are increasingly being used in pharmaceutical screening of cancer drugs as these models mirror human tumor biology and are adaptable to high throughput screening. Furthermore, studies in 3D also address clinically relevant issues such as drug and light penetration that might affect the therapeutic response of therapies such as PDT.

PDT that targets mitochondria can induce release of cytochrome c, a known trigger for apoptosis [53, 63]. Lysosomal photodamage results in release of lysosomal proteases into the cytoplasm leading to cleavage (activation) of the pro-apoptotic protein Bid and an interaction with the mitochondrial membrane that results in cytochrome c release and apoptosis [59, 72]. Photodamage to lysosomes followed by additional photodamage due to targeting mitochondria was found to promote cell death in 2D models [23]. Here we found that the combination PDT protocol eradicated IBC structures more effectively. PDT targeting lysosomes and mitochondria sequentially was also shown to be more effective in treatment of sarcomas in a mouse model [73]. Yousefi et al. [74] reported that a calpain-mediated cleavage of autophagy related protein 5 (ATG5) could amplify a pro-apoptotic signal. In accordance with this study, a recent report by Kessel et al. [75] suggests a calpain-mediated mechanism for the improved efficacy of the sequential protocol, a possibility that will be the subject of future investigations. Studies with combination PDT also suggest that before this protocol is taken to the clinic, one should consider the combinations and variations of PDT doses. In fact, a serious side effect of PDT at higher doses is partial or full thickness skin ulceration and skin necrosis. We surmise that these side effects could be reduced or eliminated using combination PDT since the overall PDT dose can be reduced without affecting the anti-tumor response.

Conclusions

Our data demonstrate the feasibility for eradication of 3D MAME structures of IBC by BPD–PDT. To our knowledge, this is the first study to show using an IBC MAME model that combinatorial targeting of lysosomes and mitochondria with PDT is significantly more efficacious than targeting mitochondria alone. Furthermore, combination PDT results in photokilling of IBC MAME structures by apoptosis as evidenced by activated caspase-3 and changes in nuclear morphology. Our study suggests that the use of PDT and in particular the lower doses made possible by the combination PDT protocol should be explored for the treatment of IBC.

Supplementary Material

Refer to Web version on PubMed Central for supplementary material.

Acknowledgments

We thank Dr. Kamiar Moin and the Microscopy, Imaging and Cytometry Resources Core at Wayne State University School for consultation and training on the use of confocal microscopes.

Funding This work was supported by National Institute of Health R01 CA131990 to BFS and CA23378 to DK. Imaging was performed in the Microscopy, Imaging and Cytometry Resources Core of Wayne State University, which was supported in part by NIH Center grant P30CA22453 to the Karmanos Cancer Institute and by the Perinatology Branch of the National Institute of Child Health and Development.

References

1. Chang S, Parker SL, Pham T, Buzdar AU, Hursting SD. Inflammatory breast carcinoma incidence and survival: the surveillance, epidemiology, and end results program of the National Cancer Institute, 1975–1992. Cancer. 1998; 82(12):2366–2372. [PubMed: 9635529]
2. Cristofanilli M, Valero V, Buzdar AU, Kau SW, Broglio KR, Gonzalez-Angulo AM, Sneige N, Islam R, Ueno NT, Buchholz TA, Singletary SE, Hortobagyi GN. Inflammatory breast cancer (IBC) and patterns of recurrence: understanding the biology of a unique disease. Cancer. 2007; 110(7): 1436–1444.10.1002/cncr.22927 [PubMed: 17694554]
3. Low JA, Berman AW, Steinberg SM, Danforth DN, Lippman ME, Swain SM. Long-term follow-up for locally advanced and inflammatory breast cancer patients treated with multimodality therapy. J Clin Oncol Off J Am Soc Clin Oncol. 2004; 22(20):4067–4074.10.1200/JCO.2004.04.068
4. van Uden DJ, van Laarhoven HW, Westenberg AH, de Wilt JH, Blanken-Peeters CF. Inflammatory breast cancer: an overview. Crit Rev Oncol/Hematol. 2015; 93(2):116–126.10.1016/j.critrevonc.2014.09.003
5. Matro JM, Li T, Cristofanilli M, Hughes ME, Ottesen RA, Weeks JC, Wong YN. Inflammatory breast cancer management in the national comprehensive cancer network: the disease, recurrence pattern, and outcome. Clin Breast Cancer. 2015; 15(1):1–7.10.1016/j.clbc.2014.05.005 [PubMed: 25034439]
6. Bertucci F, Tarpin C, Charafe-Jauffret E, Bardou VJ, Braud AC, Tallet A, Gravis G, Viret F, Goncalves A, Houvenaeghel G, Blaise D, Jacquemier J, Maraninchi D, Viens P. Multivariate analysis of survival in inflammatory breast cancer: impact of intensity of chemotherapy in multimodality treatment. Bone Marrow Transplant. 2004; 33(9):913–920.10.1038/sj.bmt.1704458 [PubMed: 15004544]
7. Lo AC, Kleer CG, Banerjee M, Omar S, Khaled H, Eissa S, Hablas A, Douglas JA, Alford SH, Merajver SD, Soliman AS. Molecular epidemiologic features of inflammatory breast cancer: a comparison between Egyptian and US patients. Breast Cancer Res Treat. 2008; 112(1):141–147.10.1007/s10549-007-9833-z [PubMed: 18058225]

8. Soliman AS, Kleer CG, Mrad K, Karkouri M, Omar S, Khaled HM, Benider AL, Ayed FB, Eissa SS, Eissa MS, McSpadden EJ, Lo AC, Toy K, Kantor ED, Xiao Q, Hampton C, Merajver SD. Inflammatory breast cancer in north Africa: comparison of clinical and molecular epidemiologic characteristics of patients from Egypt, Tunisia, and Morocco. Breast Dis. 2011; 33(4):159–169.10.3233/BD-2012-000337 [PubMed: 23001584]
9. Masuda H, Baggerly KA, Wang Y, Iwamoto T, Brewer T, Pusztai L, Kai K, Kogawa T, Finetti P, Birnbaum D, Dirix L, Woodward WA, Reuben JM, Krishnamurthy S, Symmans W, Van Laere SJ, Bertucci F, Hortobagyi GN, Ueno NT. Comparison of molecular subtype distribution in triple-negative inflammatory and non-inflammatory breast cancers. Breast Cancer Res. 2013; 15(6):R112.10.1186/bcr3579 [PubMed: 24274653]
10. Zell JA, Tsang WY, Taylor TH, Mehta RS, Anton-Culver H. Prognostic impact of human epidermal growth factor-like receptor 2 and hormone receptor status in inflammatory breast cancer (IBC): analysis of 2,014 IBC patient cases from the California Cancer Registry. Breast Cancer Res. 2009; 11(1):R9.10.1186/bcr2225 [PubMed: 19228416]
11. Zhou J, Yan Y, Guo L, Ou H, Hai J, Zhang C, Wu Z, Tang L. Distinct outcomes in patients with different molecular subtypes of inflammatory breast cancer. Saudi Med J. 2014; 35(11):1324–1330. [PubMed: 25399208]
12. Agostinis P, Berg K, Cengel KA, Foster TH, Girotti AW, Gollnick SO, Hahn SM, Hamblin MR, Juzeniene A, Kessel D, Korbelik M, Moan J, Mroz P, Nowis D, Piette J, Wilson BC, Golab J. Photodynamic therapy of cancer: an update. CA Cancer J Clin. 2011; 61(4):250–281.10.3322/caac.20114 [PubMed: 21617154]
13. Celli JP, Spring BQ, Rizvi I, Evans CL, Samkoe KS, Verma S, Pogue BW, Hasan T. Imaging and photodynamic therapy: mechanisms, monitoring, and optimization. Chem Rev. 2010; 110(5):2795–2838.10.1021/cr900300p [PubMed: 20353192]
14. Kessel D, Oleinick NL. Photodynamic therapy and cell death pathways. Methods Mol Biol. 2010; 635:35–46.10.1007/978-1-60761-697-9_3 [PubMed: 20552338]
15. Dolmans DE, Fukumura D, Jain RK. Photodynamic therapy for cancer. Nat Rev Cancer. 2003; 3(5):380–387.10.1038/nrc1071 [PubMed: 12724736]
16. Dougherty TJ, Gomer CJ, Henderson BW, Jori G, Kessel D, Korbelik M, Moan J, Peng Q. Photodynamic therapy. J Natl Cancer Inst. 1998; 90(12):889–905. [PubMed: 9637138]
17. Biel MA. Photodynamic therapy treatment of early oral and laryngeal cancers. Photochem Photobiol. 2007; 83(5):1063–1068.10.1111/j.1751-1097.2007.00153.x [PubMed: 17880501]
18. Morrison SA, Hill SL, Rogers GS, Graham RA. Efficacy and safety of continuous low-irradiance photodynamic therapy in the treatment of chest wall progression of breast cancer. J Surg Res. 2014; 192(2):235–241.10.1016/j.jss.2014.06.030 [PubMed: 25043529]
19. Allison RR, Sibata C, Mang TS, Bagnato VS, Downie GH, Hu XH, Cuenca R. Photodynamic therapy for chest wall recurrence from breast cancer. Photodiagn Photodyn Ther. 2004; 1(2):157–171.10.1016/S1572-1000(04)00039-0
20. Allison R, Mang T, Hewson G, Snider W, Dougherty D. Photodynamic therapy for chest wall progression from breast carcinoma is an underutilized treatment modality. Cancer. 2001; 91(1):1–8. [PubMed: 11148553]
21. Rogers GS. Continuous low-irradiance photodynamic therapy: a new therapeutic paradigm. J Natl Compr Cancer Netw. 2012; 10(Suppl 2):S14–S17.
22. Acedo P, Stockert JC, Canete M, Villanueva A. Two combined photosensitizers: a goal for more effective photodynamic therapy of cancer. Cell Death Dis. 2014; 5:e1122.10.1038/cddis.2014.77 [PubMed: 24625981]
23. Kessel D, Reiners JJ Jr. Enhanced efficacy of photodynamic therapy via a sequential targeting protocol. Photochem Photobiol. 2014; 90(4):889–895.10.1111/php.12270 [PubMed: 24617972]
24. Villanueva A, Stockert JC, Canete M, Acedo P. A new protocol in photodynamic therapy: enhanced tumour cell death by combining two different photosensitizers. Photochem Photobiol Sci Off J Eur Photochem Assoc Eur Soc Photobiol. 2010; 9(3):295–297.10.1039/b9pp00153k
25. Eke I, Cordes N. Radiobiology goes 3D: how ECM and cell morphology impact on cell survival after irradiation. Radiother Oncol J Eur Soc Ther Radiol Oncol. 2011; 99(3):271–278.10.1016/j.radonc.2011.06.007

26. Weigelt B, Bissell MJ. Unraveling the microenvironmental influences on the normal mammary gland and breast cancer. Semin Cancer Biol. 2008; 18(5):311–321.10.1016/j.semcancer.2008.03.013 [PubMed: 18455428]
27. Chen J, Wang J, Zhang Y, Chen D, Yang C, Kai C, Wang X, Shi F, Dou J. Observation of ovarian cancer stem cell behavior and investigation of potential mechanisms of drug resistance in three-dimensional cell culture. J Biosci Bioeng. 2014; 118(2):214–222.10.1016/j.jbiosc.2014.01.008 [PubMed: 24684961]
28. Li Q, Chow AB, Mattingly RR. Three-dimensional overlay culture models of human breast cancer reveal a critical sensitivity to mitogen-activated protein kinase kinase inhibitors. J Pharmacol Exp Ther. 2010; 332(3):821–828.10.1124/jpet.109.160390 [PubMed: 19952304]
29. Storch K, Eke I, Borgmann K, Krause M, Richter C, Becker K, Schrock E, Cordes N. Three-dimensional cell growth confers radioresistance by chromatin density modification. Cancer Res. 2010; 70(10):3925–3934.10.1158/0008-5472.CAN-09-3848 [PubMed: 20442295]
30. Rizvi I, Anbil S, Alagic N, Celli J, Zheng LZ, Palanisami A, Glidden MD, Pogue BW, Hasan T. PDT dose parameters impact tumoricidal durability and cell death pathways in a 3D ovarian cancer model. Photochem Photobiol. 2013; 89(4):942–952.10.1111/php.12065 [PubMed: 23442192]
31. Celli JP, Solban N, Liang A, Pereira SP, Hasan T. Verteporfin-based photodynamic therapy overcomes gemcitabine insensitivity in a panel of pancreatic cancer cell lines. Lasers Surg Med. 2011; 43(7):565–574.10.1002/lsm.21093 [PubMed: 22057484]
32. Anbil S, Rizvi I, Celli JP, Alagic N, Pogue BW, Hasan T. Impact of treatment response metrics on photodynamic therapy planning and outcomes in a three-dimensional model of ovarian cancer. J Biomed Opt. 2013; 18(9):098004.10.1117/1.JBO.18.9.098004 [PubMed: 24802230]
33. Osuala KO, Sameni M, Shah S, Aggarwal N, Simonait ML, Franco OE, Hong Y, Hayward SW, Behbod F, Mattingly RR, Sloane BF. Il-6 signaling between ductal carcinoma in situ cells and carcinoma-associated fibroblasts mediates tumor cell growth and migration. BMC Cancer. 2015; 15:584.10.1186/s12885-015-1576-3 [PubMed: 26268945]
34. Rothberg JM, Bailey KM, Wojtkowiak JW, Ben-Nun Y, Bogyo M, Weber E, Moin K, Blum G, Mattingly RR, Gillies RJ, Sloane BF. Acid-mediated tumor proteolysis: contribution of cysteine cathepsins. Neoplasia. 2013; 15(10):1125–1137. [PubMed: 24204192]
35. Mullins SR, Sameni M, Blum G, Bogyo M, Sloane BF, Moin K. Three-dimensional cultures modeling premalignant progression of human breast epithelial cells: role of cysteine cathepsins. Biol Chem. 2012; 393(12):1405–1416.10.1515/hsz-2012-0252 [PubMed: 23667900]
36. Sameni M, Anbalagan A, Olive MB, Moin K, Mattingly RR, Sloane BF. MAME models for 4D live-cell imaging of tumor: microenvironment interactions that impact malignant progression. J Vis Exp. 2012; 60:e3661.10.3791/3661
37. Moin K, Sameni M, Victor BC, Rothberg JM, Mattingly RR, Sloane BF. 3D/4D functional imaging of tumor-associated proteolysis: impact of microenvironment. Methods Enzymol. 2012; 506:175–194.10.1016/B978-0-12-391856-7.00034-2 [PubMed: 22341225]
38. Victor BC, Anbalagan A, Mohamed MM, Sloane BF, Cavallo-Medved D. Inhibition of cathepsin B activity attenuates extracellular matrix degradation and inflammatory breast cancer invasion. Breast Cancer Res. 2011; 13(6):R115.10.1186/bcr3058 [PubMed: 22093547]
39. Jedeszko C, Victor BC, Podgorski I, Sloane BF. Fibroblast hepatocyte growth factor promotes invasion of human mammary ductal carcinoma in situ. Cancer Res. 2009; 69(23):9148–9155.10.1158/0008-5472.CAN-09-1043 [PubMed: 19920187]
40. Weaver VM, Bissell MJ. Functional culture models to study mechanisms governing apoptosis in normal and malignant mammary epithelial cells. J Mammary Gland Biol Neoplas. 1999; 4(2):193–201.
41. Bissell MJ, Weaver VM, Lelievre SA, Wang F, Petersen OW, Schmeichel KL. Tissue structure, nuclear organization, and gene expression in normal and malignant breast. Cancer research. 1999; 59(7 Suppl):1757–1763s. discussion 1763 s-1764 s. [PubMed: 10197593]
42. Howlett AR, Bissell MJ. The influence of tissue microenvironment (stroma and extracellular matrix) on the development and function of mammary epithelium. Epithel Cell Biol. 1993; 2(2):79–89.

43. Debnath J, Brugge JS. Modelling glandular epithelial cancers in three-dimensional cultures. Nat Rev Cancer. 2005; 5(9):675–688.10.1038/nrc1695 [PubMed: 16148884]
44. Debnath J, Mills KR, Collins NL, Reginato MJ, Muthuswamy SK, Brugge JS. The role of apoptosis in creating and maintaining luminal space within normal and oncogene-expressing mammary acini. Cell. 2002; 111(1):29–40. [PubMed: 12372298]
45. Sameni M, Dosescu J, Yamada KM, Sloane BF, Cavallo-Medved D. Functional live-cell imaging demonstrates that beta1-integrin promotes type IV collagen degradation by breast and prostate cancer cells. Mol Imaging. 2008; 7(5):199–213. [PubMed: 19123990]
46. Celli JP, Rizvi I, Blanden AR, Massodi I, Glidden MD, Pogue BW, Hasan T. An imaging-based platform for high-content, quantitative evaluation of therapeutic response in 3D tumour models. Sci Rep. 2014; 4:3751.10.1038/srep03751 [PubMed: 24435043]
47. Lehmann BD, Bauer JA, Chen X, Sanders ME, Chakravarthy AB, Shyr Y, Pietenpol JA. Identification of human triple-negative breast cancer subtypes and preclinical models for selection of targeted therapies. J Clin Investig. 2011; 121(7):2750–2767.10.1172/JCI45014 [PubMed: 21633166]
48. Guelfi MR, Masoni M, Torelli G, Fonda S, Caramella D. A proposal for the use of tridimensional reconstruction in oncology to better assess tumor stage and response to therapy. Radiol Med (Torino). 1994; 87(5):669–676. [PubMed: 7516562]
49. Edgerton ME, Chuang YL, Macklin P, Yang W, Bearer EL, Cristini V. A novel, patient-specific mathematical pathology approach for assessment of surgical volume: application to ductal carcinoma in situ of the breast. Anal Cell Pathol. 2011; 34(5):247–263.10.3233/ACP-2011-0019
50. Mozley PD, Schwartz LH, Bendtsen C, Zhao B, Petrick N, Buckler AJ. Change in lung tumor volume as a biomarker of treatment response: a critical review of the evidence. Ann Oncol Off J Eur Soc Med Oncol/ESMO. 2010; 21(9):1751–1755.10.1093/annonc/mdq051
51. Mukherji SK, Schmalfuss IM, Castelijns J, Mancuso AA. Clinical applications of tumor volume measurements for predicting outcome in patients with squamous cell carcinoma of the upper aerodigestive tract. AJNR Am J Neuroradiol. 2004; 25(8):1425–1432. [PubMed: 15466346]
52. Lee CC, Huang TT, Lee MS, Hsiao SH, Lin HY, Su YC, Hsu FC, Hung SK. Clinical application of tumor volume in advanced nasopharyngeal carcinoma to predict outcome. Radiat Oncol. 2010; 5:20.10.1186/1748-717X-5-20 [PubMed: 20222940]
53. Kessel D, Luo Y. Mitochondrial photodamage and PDT-induced apoptosis. J Photochem Photobiol, B, Biol. 1998; 42(2):89–95.
54. Kessel D, Reiners JJ Jr. Apoptosis and autophagy after mitochondrial or endoplasmic reticulum photo damage. Photochem Photobiol. 2007; 83(5):1024–1028.10.1111/j.1751-1097.2007.00088.x [PubMed: 17880495]
55. Agarwal ML, Clay ME, Harvey EJ, Evans HH, Antunez AR, Oleinick NL. Photodynamic therapy induces rapid cell death by apoptosis in L5178Y mouse lymphoma cells. Cancer Res. 1991; 51(21):5993–5996. [PubMed: 1933862]
56. Diamond I, Granelli SG, McDonagh AF, Nielsen S, Wilson CB, Jaenicke R. Photodynamic therapy of malignant tumours. Lancet. 1972; 2(7788):1175–1177. [PubMed: 4117595]
57. Andrzejak M, Price M, Kessel DH. Apoptotic and autophagic responses to photodynamic therapy in 1c1c7 murine hepatoma cells. Autophagy. 2011; 7(9):979–984. [PubMed: 21555918]
58. Kessel D, Luo Y, Mathieu P, Reiners JJ Jr. Determinants of the apoptotic response to lysosomal photodamage. Photochem Photobiol. 2000; 71(2):196–200. [PubMed: 10687394]
59. Reiners JJ Jr, Caruso JA, Mathieu P, Chelladurai B, Yin XM, Kessel D. Release of cytochrome c and activation of procaspase-9 following lysosomal photodamage involves Bid cleavage. Cell Death Differ. 2002; 9(9):934–944.10.1038/sj.cdd.4401048 [PubMed: 12181744]
60. Kerr JF, Wyllie AH, Currie AR. Apoptosis: a basic biological phenomenon with wide-ranging implications in tissue kinetics. Br J Cancer. 1972; 26(4):239–257. [PubMed: 4561027]
61. Kerr JF. History of the events leading to the formulation of the apoptosis concept. Toxicology. 2002; 181–182:471–474.
62. Wyllie AH, Kerr JF, Currie AR. Cell death: the significance of apoptosis. Int Rev Cytol. 1980; 68:251–306. [PubMed: 7014501]

63. Granville DJ, Carthy CM, Jiang H, Shore GC, McManus BM, Hunt DW. Rapid cytochrome c release, activation of caspases 3, 6, 7 and 8 followed by Bap31 cleavage in HeLa cells treated with photodynamic therapy. FEBS Lett. 1998; 437(1–2):5–10. [PubMed: 9804161]
64. Janicke RU, Sprengart ML, Wati MR, Porter AG. Caspase-3 is required for DNA fragmentation and morphological changes associated with apoptosis. J Biol Chem. 1998; 273(16):9357–9360. [PubMed: 9545256]
65. Porter AG, Janicke RU. Emerging roles of caspase-3 in apoptosis. Cell Death Differ. 1999; 6(2): 99–104.10.1038/sj.cdd.4400476 [PubMed: 10200555]
66. Renehan AG, Booth C, Potten CS. What is apoptosis, and why is it important? BMJ. 2001; 322(7301):1536–1538. [PubMed: 11420279]
67. Ding X, Xu Q, Liu F, Zhou P, Gu Y, Zeng J, An J, Dai W, Li X. Hematoporphyrin monomethyl ether photodynamic damage on HeLa cells by means of reactive oxygen species production and cytosolic free calcium concentration elevation. Cancer Lett. 2004; 216(1):43–54.10.1016/j.canlet.2004.07.005 [PubMed: 15500948]
68. Henderson BW, Donovan JM. Release of prostaglandin E2 from cells by photodynamic treatment in vitro. Cancer Res. 1989; 49(24 Pt 1):6896–6900. [PubMed: 2531034]
69. Dahle J, Kaalhus O, Moan J, Steen HB. Cooperative effects of photodynamic treatment of cells in microcolonies. Proc Natl Acad Sci USA. 1997; 94(5):1773–1778. [PubMed: 9050854]
70. Dahle J, Bagdonas S, Kaalhus O, Olsen G, Steen HB, Moan J. The bystander effect in photodynamic inactivation of cells. Biochim Biophys Acta. 2000; 1475(3):273–280. [PubMed: 10913826]
71. Dawood S, Ueno NT, Valero V, Woodward WA, Buchholz TA, Hortobagyi GN, Gonzalez-Angulo AM, Cristofanilli M. Identifying factors that impact survival among women with inflammatory breast cancer. Ann Oncol Off J Eur Soc Med Oncol/ESMO. 2012; 23(4):870–875.10.1093/annonc/mdr319
72. Kessel D, Poretz RD. Sites of photodamage induced by photodynamic therapy with a chlorin e6 triacetoxymethyl ester (CAME). Photochem Photobiol. 2000; 71(1):94–96. [PubMed: 10649895]
73. Cincotta L, Szeto D, Lampros E, Hasan T, Cincotta AH. Benzophenothiazine and benzoporphyrin derivative combination phototherapy effectively eradicates large murine sarcomas. Photochem Photobiol. 1996; 63(2):229–237. [PubMed: 8657737]
74. Yousefi S, Perozzo R, Schmid I, Ziemiecki A, Schaffner T, Scapozza L, Brunner T, Simon HU. Calpain-mediated cleavage of Atg5 switches autophagy to apoptosis. Nat Cell Biol. 2006; 8(10): 1124–1132.10.1038/ncb1482 [PubMed: 16998475]
75. Kessel D, Reiners JJ Jr. Promotion of Proapoptotic Signals by Lysosomal Photodamage. Photochem Photobiol. 2015; 91(4):931–936.10.1111/php.12456 [PubMed: 25873082]

Abbreviations

IBC	Inflammatory breast cancer
ECM	Extracellular matrix
rBM	Reconstituted basement membrane
2D	2-dimensional
3D	3-dimensional
PDT	Photodynamic therapy
BPD	Benzoporphyrin derivative monoacid A
NPe6	*N*-aspartyl chlorin e6
MAME	Mammary architecture and microenvironment engineering

MEGM Mammary epithelial cell growth medium

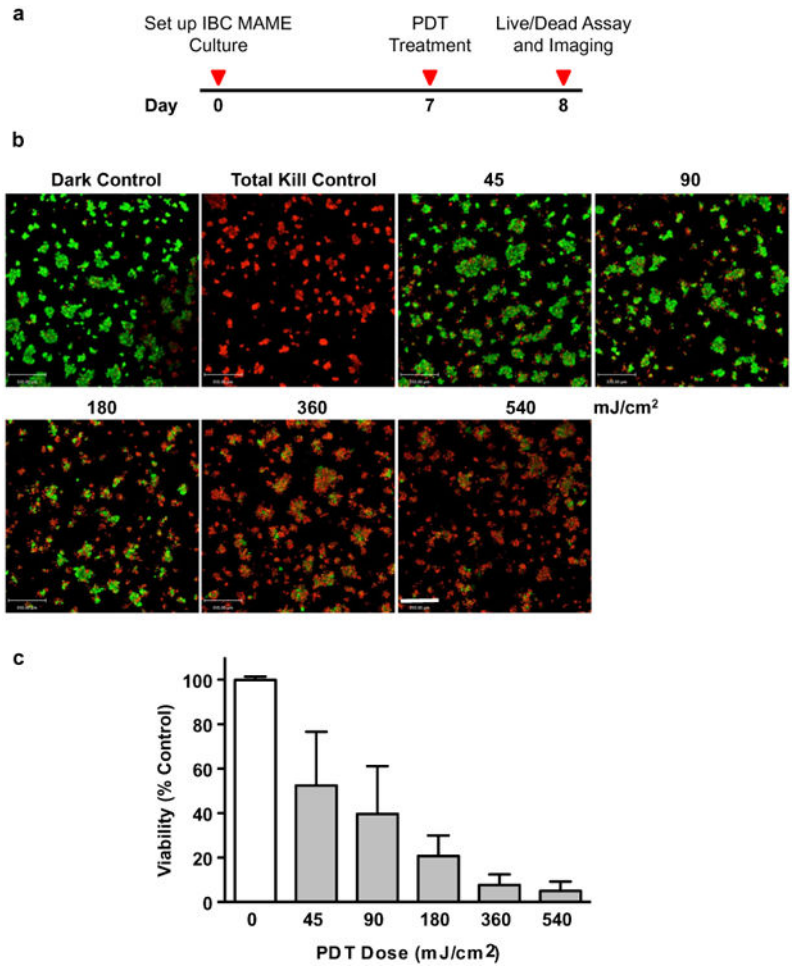

Fig. 1.

BPD–PDT induces dose-dependent photokilling of SUM149 cells in MAME cultures. Timeline shows events during PDT of MAME cultures (**a**). Tiled 16-panel images and z-stacks through the depth of structures were captured and reconstructed in 3D to show an *en face* view (**b**). Images show live cells (*green*, calcein AM) and dead cells (*red*, ethidium homodimer-1) and were taken 24 h after PDT with 1.5 μM BPD and for untreated dark control; *scale bar* equals 350 microns. Intensities of *red* (dead) and *green* (live) fluorescence were used to calculate viability that is plotted against PDT dose (**c**). Significance was calculated by one-way ANOVA, p-value <0.0001; $n = 8$, mean ± SD

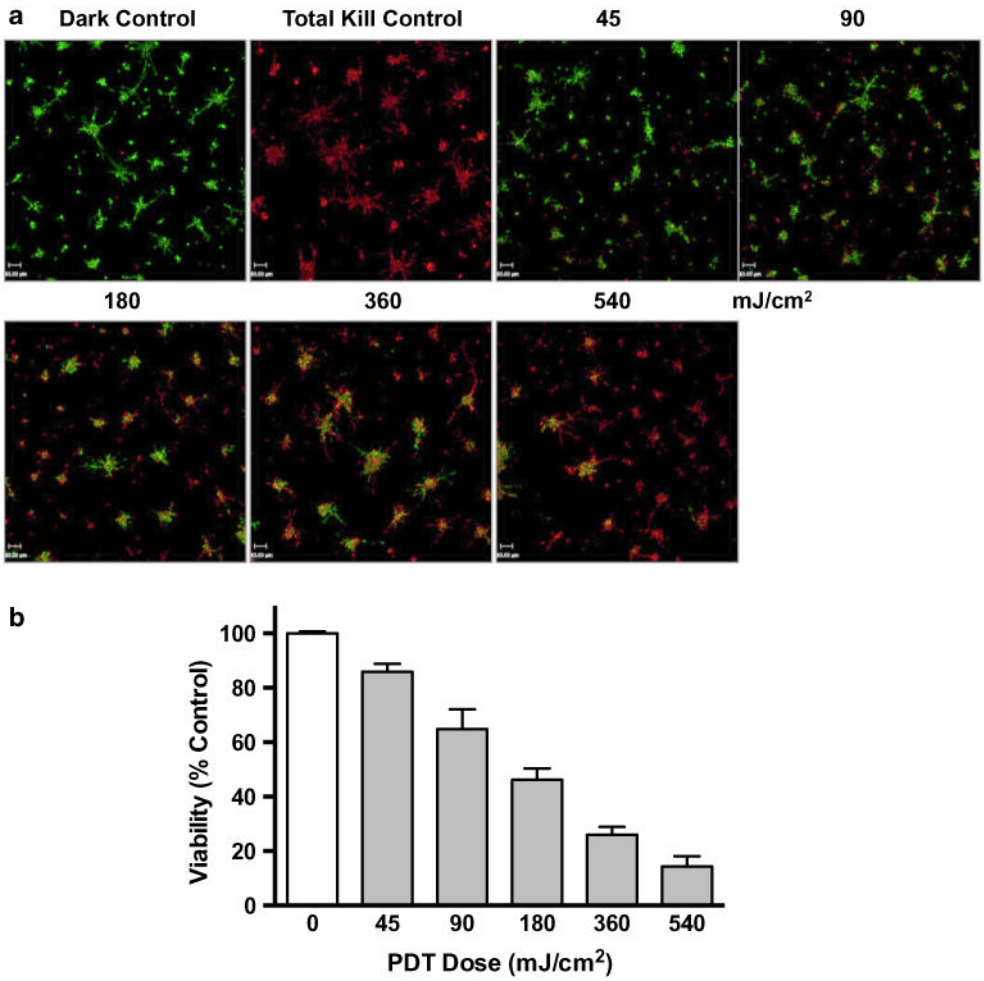

Fig. 2.

BPD–PDT induces dose-dependent photokilling of MAME structures of MDA-MB-231 cells. Tiled 16-panel images and z-stacks through the depth of structures were captured and reconstructed in 3D to show an *en face* view (**a**). Images show live cells (*green*, calcein AM) and dead cells (*red*, ethidium homodimer-1) and were taken 24 h after PDT with 1.5 μM BPD and for untreated dark control; *scale bar* equals 700 microns. Intensities of *red* (dead) and *green* (live) fluorescence were used to calculate viability that is plotted against PDT dose (**b**). Significance was calculated by one-way ANOVA, p-value <0.0001; $n = 6$, mean ± SD

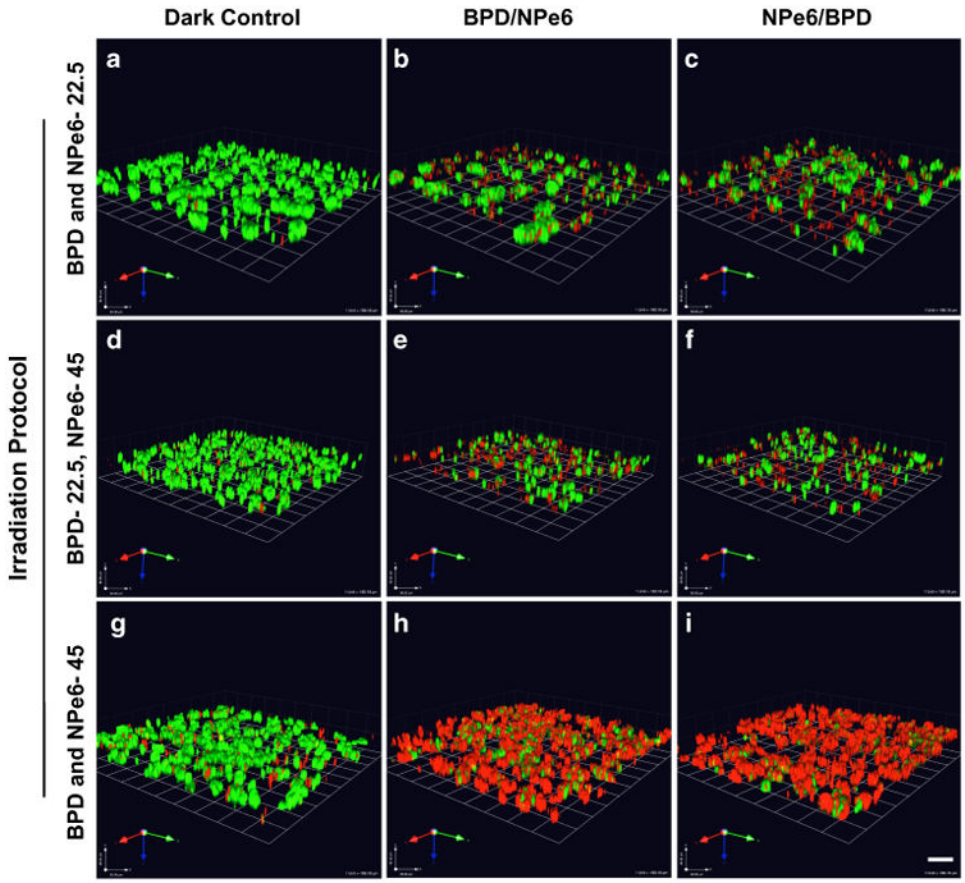

Fig. 3.

Combination PDT promotes photokilling of SUM149 cells in MAME cultures. Optical sections through the depth of 3D structures were captured for 16 contiguous fields 24 h after therapy and reconstructed in 3D. Representative images show live cells (*green*, calcein AM) and dead cells (*red*, ethidium homodimer-1) for untreated dark control (**a**, **d**, **g**); light irradiation targeting mitochondria (BPD-690 nm) and lysosomes (NPe6-660 nm) at dose of 22.5 mJ/cm^2 each (**b**, **c**); PDT targeting mitochondria (BPD) at dose of 22.5 mJ/cm^2 and lysosomes (NPe6) at dose of 45 mJ/cm^2 (**e**, **f**); and PDT targeting mitochondria (BPD) and lysosomes (NPe6) at dose of 45 mJ/cm^2 each (**h**, **i**); *scale bar* equals 80 microns

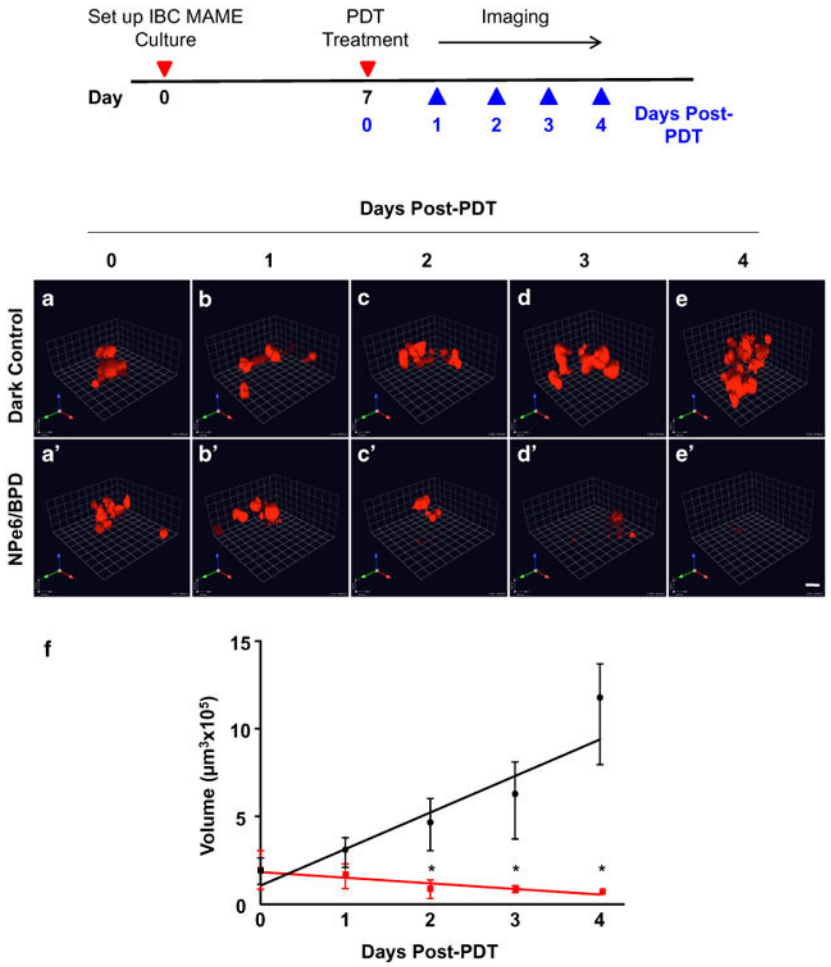

Fig. 4.

SUM149 structure volume assesses phenotypic response to the sequential PDT protocol. Schematic shows events during treatment and assessment of response to treatment. Representative 3D images of SUM149-RFP cells in MAME cultures (*red*) treated with sequential PDT (NPe6 followed by BPD at 22.5 mJ/cm^2) (**a′**–**e′**) or untreated dark control (**a**–**e**) over 5 days after PDT: day 0 (**a**, **a′**), day 1 (**b**, **b′**), day 2 (**c**, **c′**), day 3 (**d**, **d′**), and day 4 (**e**, **e′**); *scale bars* equal 80 microns. The volume of structures was calculated using Volocity and is plotted against days post-treatment (**f**); untreated dark control (*red line*), NPe6/BPD–PDT (*black line*). Significance was calculated by two-way ANOVA. * *p*-value <0.0001, *n* = 20, mean ± SD

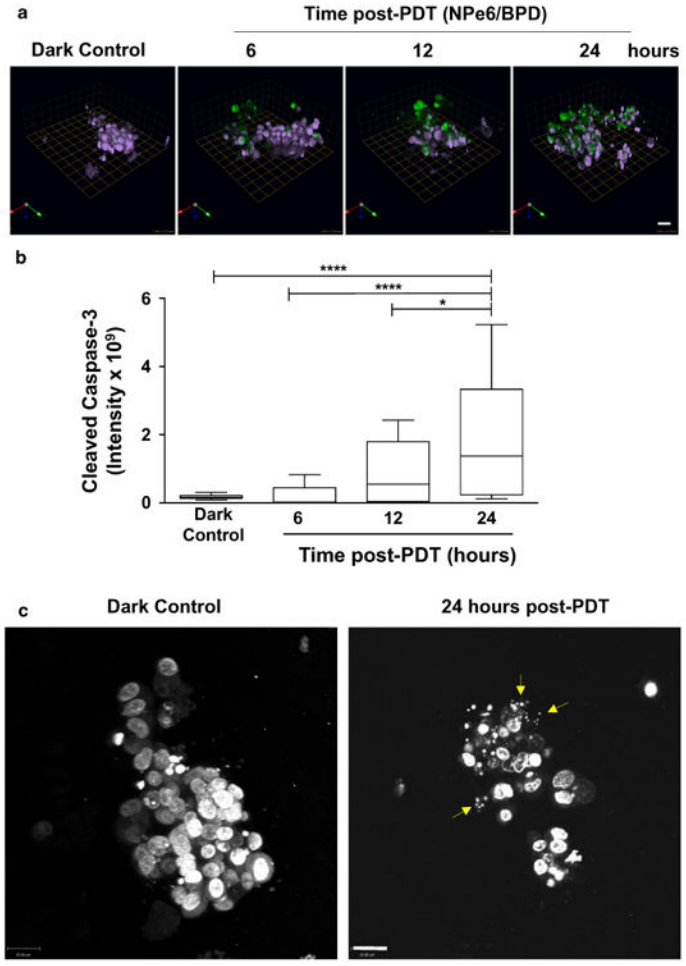

Fig. 5.

Mechanism of cell death following sequential PDT protocol is apoptosis. Panel A shows representative images of expression of cleaved caspase-3 in response to the sequential PDT protocol PDT or a dark control. Images through the depth of structures were captured at 6, 12 and 24 h after treatment and images were reconstructed in 3D using Volocity; each square unit equals 22.59 microns. *Green* florescence represents cleaved caspase-3 and *purple* represents nuclei (*pseudocolored*, Hoechst). Fluorescent intensity was quantified using Volocity and plotted against treatment (**b**); significance was calculated by ANOVA followed by Tukey's post hoc analysis. * p-value <0.05, **** p-value <0.0001, n = 20, mean ± SD. Representative images showing fragmented nuclei (*yellow arrows*) stained with Hoechst (*gray scale*) 24 h after sequential PDT protocol compared to intact nuclei for dark control (**c**); images show an *en face* view of single 3D structure and scale bars equal 22 microns

Table 1

Viability (% control) of 3D structures in response to BPD–PDT

BPD-dose (mJ/cm^2)	Dark control	45	90	180	360	540
Viability (% control)	100 ± 2	52 ± 15	40 ± 14	21 ± 6	8 ± 3	5 ± 3

Table 2

Viability (% control) of 3D structures in response to combination PDT

Treatment	Irradiation (nm)	690 nm-22.5 mJ/cm^2, 660–22.5 mJ/cm^2	690 nm-22.5 mJ/cm^2, 660–45 mJ/cm^2	690 nm-45 mJ/cm^2, 660–45 mJ/cm^2
BPD	690	80 ± 8	89 ± 10	64 ± 9
NPe6	660	95 ± 4	73 ± 22	56 ± 14
BPD and NPe6	690 » » 660	65 ± 16	40 ± 19	19 ± 13
BPD and NPe6	660 » » 690	43 ± 9	40 ± 25	6 ± 4